https://doi.org/10.5194/egusphere-2026-3415
Preprint. Discussion started: 3 July 2026

Midlatitude cooling across the Oligocene-Miocene transition

Thomas Tanner[1], Iván Hernández-Almeida[1], Reto Wijker[1], Andrea K. Manirajan[1], Madeleine Santos[1], Peter Bijl[2], Tim van Peer[3], and Heather Stoll[1]

[1]Department of Earth Sciences, ETH Zürich, Sonneggstrasse 5, 8092 Zürich, Switzerland
2 Utrecht University
3 School of Geography, Geology and the Environment, University of Leicester, University Road, LE1 7RH, Leicester, United Kingdom

Correspondence to: Heather M. Stoll (heather.stoll@eaps.ethz.ch)

Abstract

The transition from the Oligocene into the Miocene is marked by a significant positive benthic $\delta^{18}O$ excursion, the Mi-1, which is interpreted to reflect a transient period of Antarctic ice sheet growth. Despite an increasing number of orbitally resolved benthic records reflecting deep ocean conditions, few comparable high-resolution records exist to evaluate whether this event also entailed changes in surface ocean temperatures either regionally in the Southern Ocean or globally. Here, we aim to evaluate the timing and amplitude of changes in surface ocean temperatures. We present new alkenone undersaturation temperatures from a site in the Southern Ocean on the Tasman Rise (ODP Site 1168), as well as from a site in the North Atlantic on the Newfoundland Margin (IODP Site U1406). Our results show a nearly 4°C cooling in the Southern Ocean between 24 and 23 Ma in two steps.When benthic $\delta^{18}O$ recovers to the lower values typical of the pre- Mi-1 excursion, there is only limited warming in average temperature between 23 and 22 Ma. In the North Atlantic our sampling captures only the second step of 2°C cooling between 23.4 and 23.0 Ma, and average temperatures recover by nearly 2°C by 22 Ma. These results suggest a consistent cooling of SST in both hemispheres during the Mi-1 glaciation. Bulk carbonate $\delta^{18}O$ records from Site U1406 shows similar magnitude and timing of change as benthic $\delta^{18}O$ from the site, and bulk carbonate from Site 1168 shows similar magnitude and timing of change as the deep South Atlantic Site 1264. Additionally, we generate surface ocean $\delta^{18}O_{sw}$ estimates from alkenone SST and coccolith dominated bulk carbonate $\delta^{18}O$ for both sites. Comparison of these estimates with benthic $\delta^{18}O$ is consistent with significant deep ocean cooling during both the Mi-1 and Mi-1.1 (22.5 Ma) glacial intervals. Together, these records indicate that Mi-1 was associated with coherent surface ocean cooling across both hemispheres, supporting a tightly coupled response of the surface ocean, deep ocean, and Antarctic cryosphere during this major glaciation.

1 Introduction

The Oligocene to Miocene transition (OMT) at 23.03 Ma marks the culmination of a ~1‰ extreme positive excursion in the $\delta^{18}O_{benthic}$, recognized as the Mi-1 glaciation (after(Miller et al., 1991), a ~300 kyr-long glaciation of Antarctica (Naish et al., 2022) which saw the first major ice sheet expansion across the Ross Sea continental shelf(Levy et al., 2019). The OMT is suggested to entail ~50 m of sea-level fall(Beddow et al., 2016). The intensified glaciation of the OMT coincides with a minimum in the 405 kyr-long eccentricity cycle and a 1.2 Myr-paced minimum in the amplitude variability of Earth's axial tilt (obliquity). This astronomical configuration favors ice growth at high latitudes due to the reduction of seasonality and supports an increased likelihood of winter snowfall surviving the summer ablation season, resulting in an ice build-up phase(Coxall et al., 2005; Pälike et al., 2006; Zachos et al.,

https://doi.org/10.5194/egusphere-2026-3415
Preprint. Discussion started: 3 July 2026

2001). Both short eccentricity and obliquity components are present in the $\delta^{18}O_{benthic}$ signal and have variable power in different deep ocean sites(Liebrand et al., 2016; Pälike et al., 2006; Van Peer et al., 2024).

However, in addition to ice volume changes, changes in the deep-ocean temperature may also contribute significantly to the $\delta^{18}O_{benthic}$ variability. It is proposed that variation in bottom-water temperatures may itself be driven by changes in the areal extent of the Antarctic ice sheet (AIS) via surface albedo(Bradshaw et al., 2021). Recent comparison of results from a wide range of atmosphere-ocean general circulation models (AOGCM) suggests that deep ocean temperature closely tracks earth's mean annual surface temperature(Evans et al., 2024). Compilation of surface ocean temperature records can help test the relationships between earth surface temperature, deep ocean temperature, and Antarctic expansions over the OMT. However, because of high-amplitude astronomical variations during the late Oligocene and early Miocene, it is difficult to compare high and middle latitude surface ocean temperature records with the benthic record as there is significant potential for aliasing of temperature trends when climate variables are sampled at lower resolution than astronomical variability. Adequately addressing this challenge requires high temporal resolution records of surface ocean conditions.

In this study, we provide a new, high resolution (~10 kyr resolution) alkenone sea surface temperature (SST) and coccolith fraction $\delta^{18}O$ record from two sites, Site 1168 in the Tasmanian Margin in the southern hemisphere and Site U1406 in the Newfoundland Margin in the northern hemisphere, covering the interval between ~24 and 22.5 Ma. Existing SST records from both regions for the time interval are at much lower temporal resolution(Guitián et al., 2019; Liu et al., 2018; Śliwińska et al., 2014). Therefore, with this record we can evaluate the surface ocean temperature trends leading into and out of the extreme $\delta^{18}O_{benthic}$ maximum of the OMT, and during the strong 110 kyr cycles in $\delta^{18}O_{benthic}$ of the latter half of the OMT. We also evaluate the changes in the local $\delta^{18}O_{sw}$ during the OMT from the paired $\delta^{18}O_{bulk}$ and alkenone temperatures which are derived from the dominant coccolith producing genera.

2 Palaeoceanographic setting

2.1 Site 1168

ODP Site 1168 (42°37' S, 144°25' E) recovered during Leg 189 is located at the western continental margin of Tasmania (Fig. 1) at a present water depth of 2463 m, north of the Subtropical Front (STF). Due to its proximity to land, sedimentation rates between 2-6 cm/kyr are observed within the interval of the OMT(Exon et al., 2001). The reconstructed paleo-location for Site 1168 for the time of the OMT is further south at around 53°43' S, 143°10' E, lying in the southwest Pacific sector of the Southern Ocean(Kim and Zhang, 2022). The paleo-water depth ranges between ~500 and 1500 m and is mainly based on microfossil and sedimentary facies analysis(Pfuhl et al., 2004). A deepening from about 700 m at 29 Ma to a depth of 1500 m by 21 Ma due to the opening of the Tasmanian gateway is proposed(Hochmuth et al., 2020), which caused a northward movement of Australia and a deepening of the Tasmanian continental flanks throughout the Eocene-Oligocene(Cande and Stock, 2004; Hoem et al., 2021a). In turn, this contributed to increased polar isolation of Antarctica with a strengthened proto-Antarctic Circumpolar Current (proto-ACC) deflecting the warm poleward extension of subpolar gyres away from Antarctica and hence reducing the heat transport towards the Antarctic Margin. The neodymium isotope ratio of bottom water-formed authigenic oxides in sediments from Site 1168 suggest that there was already exchange of deep waters with the Pacific and Indian basins in the late Oligocene(Scher et al., 2015).

Recent reconstructions of paleo-sea surface temperatures to evaluate the strength and variability of the Oligocene Southern Ocean (Hoem et al., 2022) and its evolution over the Neogene (Hou et al., 2022) suggest warm surface

https://doi.org/10.5194/egusphere-2026-3415
Preprint. Discussion started: 3 July 2026

ocean temperatures interpreted as evidence for continuous influence of the eastward flowing proto-Leeuwin Current (proto-LC). Previous alkenone undersaturation indices imply average temperatures of ~25.5°C during the period from 24 to 22 Ma(Guitián and Stoll, 2021). Although deep water circulation patterns are not well constrained in the latest Oligocene and earliest Miocene, most evidence suggests that deep water formation was strongest in the Southern Ocean with only limited North Atlantic deep-water formation(Steinthorsdottir et al., 2021; Thomas and Via, 2007). During the Oligocene, deep-water formation and downwelling around Antarctica might be induced by seasonal changes in SST and salinity (Goldner et al., 2014; Lunt et al., 2010) or in southerly positioned basins such as the Ross Sea, where glaciers extend onto the Antarctic shelf(Hartman et al., 2018; Sorlien et al., 2007). At the same time, variations in deepwater circulation sources or intensity in the late Oligocene have been proposed based on variable carbonate preservation in sediments from offshore Wilkes Land(Salabarnada et al., 2018).

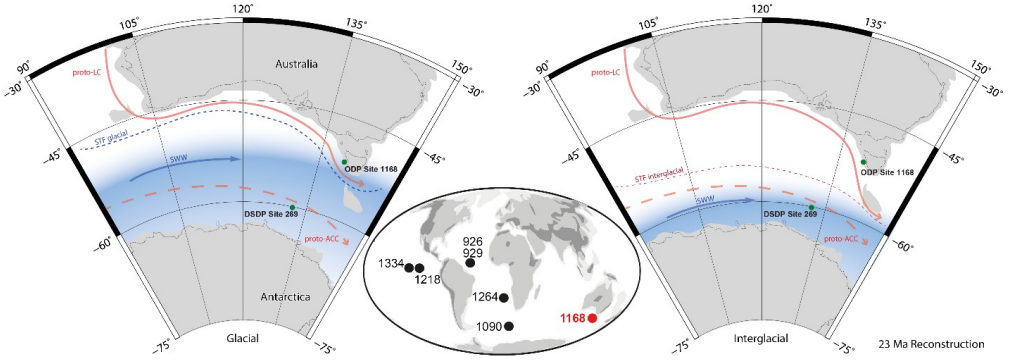

Figure 1. Reconstruction of the Southern Ocean during the OMT around 23 Ma. Highlighted are the surface proto-Leeuwin Current and the proto-Antarctic Circumpolar Current, after (Hou et al., 2022) and an overview of the different deep ocean sites referenced from (Beddow et al., 2016) in a small window. In blue is the schematic position of the Southern Westerlies (SWW) during glacial-interglacial periods. The glacial section on the left illustrates a northward expanded subtropical front (STF), which also produces a northward movement of the SWW and results in local changes in evaporation and precipitation and/or changes in advection and upwelling of water. The interglacial section on the right illustrates the opposite with SWW closer to the Antarctic continent. Reconstruction was made using the plate tectonic reconstruction service ODSN (www.odsn.de).

2.2 Site U1406

IODP Site U1406 (40˚21′ N, 51˚39′ W) was recovered from the southeast coast of Newfoundland, Canada (Fig. 2). It occupies a central position within the Expedition 342 depth transect, situated at a present water depth of 3800 m. The paleolatitude of Site U1406 has shifted little latitudinally over the studied period, according to site backtracking estimates by(Liu et al., 2018). The modern position of Site U1406 sits at the border between different surface-water environments, such as the warm Subtropical Gyre (STG) and the Gulf Stream in the south and the Arctic Front (AF) and the cold (proto-) Labrador Current in the north. The recovered sediments feature a high accumulation rate and remarkable preservation of microfossils attributed to the abundant clay content(Norris et al., 2014). Most of these sequences constitute contourite drift deposits, which extend over hundreds of kilometers and exceed 2000 m in thickness, and formed at a paleodepth of approximately 3500–4500 m on the Southeast Newfoundland Ridge. Such drift deposits have also been described in a broader region across the North Atlantic during the Late Oligocene to the Miocene-Pliocene period(Boyle et al., 2017).

https://doi.org/10.5194/egusphere-2026-3415
Preprint. Discussion started: 3 July 2026

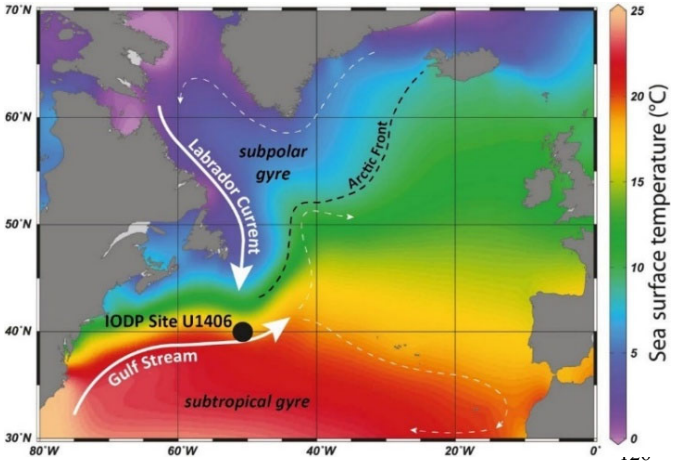

Figure 2. Present-day location of IODP Site U1406 in offshore Newfoundland. White arrows show the general circulation of major surface currents in the subtropical and subpolar gyre systems with the Gulf Stream and Labrador Current directly influencing the location. The map follows illustration from(Egger et al., 2018), who compiled the data using Ocean Data View(Schlitzer, 2017).

During the late Oligocene to early Miocene, the high accumulation rates of drift sediments make Site U1406 ideal for studies related to suborbital-scale variability(Norris et al., 2014). Moreover, it has been proposed that the high primary productivity in the overlying waters limit the significance of any biomarkers that might have been laterally transported from more distant regions(Guitián et al., 2019). Alkenone-based SSTs at Site U1406 show a shift towards warmer temperatures from 24 to 30°C during the late Oligocene-early Miocene (from 34 to 20 Ma)(Guitián et al., 2019), similar to the neighboring Site U1404, which shows a shift from 24 to 28°C over the same interval(Liu et al., 2018).

3 Methods

3.1 Sample selection and approach for age model development

3.1.1 Site 1168

ODP Site 1168 Hole A Core Sections 37X-1 through to 52X-6 were sampled for stable isotopes on bulk carbonate every 30 to 40 cm as small volume samples (366 samples). This encompasses the interval between 320 and 480 meters below sea floor (mbsf). For organic geochemistry and foraminiferal isotopes as well as bulk carbonate isotopes, Core Sections 41X-1 through to to 50X-2 were sampled at a spacing of 0.2 to 1.3 m (168 samples). Most previous palaeoceanographic studies at this site (Guitián and Stoll, 2021; Hoem et al., 2022; Hou et al., 2022; Kim and Zhang, 2022) have relied on the shipboard biostratigraphy and magnetostratigraphic reversals(Pfuhl and Mccave, 2003; Stickley et al., 2004). Due to weak magnetic intensity, identification of magnetostratigraphic reversals was most robust in Hole A between 252.60 (top of Chron C5Cn) and 347.30 mbsf (base of Chron C6n) (Exon et al., 2001)but nonetheless updated magnetostratigraphic syntheses excluded the Miocene due to uncertainties(Fuller and Touchard, 2004). Due to provincialism, biodatums featured disagreement and previous studies provide a tentative assignment of the OMT at 440 mbsf based on the last occurrence (LO) of the nannofossil *Reticulofenestra bisecta bisecta(Stickley et al., 2004)*.

Given these uncertainties in biostratigraphy and magnetostratigraphy, we devise the initial age model based on published Sr isotope stratigraphy (Stoll et al., 2024) carried out in the age-modelling software Bacon, as implemented in the rbacon package (Blaauw and Christen, 2011) in R. Within the 95% confidence interval generated by Bacon from these tie points, we further refine the age model using tie points based on tuning local maxima in $\delta^{18}O_{bulk}$ to maxima in $\delta^{18}O_{benthic}$ from ODP Site 1264 over eccentricity cycles (Supplemental Table 1). $\delta^{18}O_{bulk}$ was used for tuning because it is the highest resolution data available for the studied interval in Site 1168. This tuning strategy is based on the proposal that $\delta^{18}O_{benthic}$ of Site 1264 and the $\delta^{18}O_{bulk}$ at Site 1168 contain a common, in-phase component

https://doi.org/10.5194/egusphere-2026-3415
Preprint. Discussion started: 3 July 2026

of variation due to ice volume and that any temperature component in the $\delta^{18}O_{benthic}$ record is in phase with temperature component in the $\delta^{18}O_{bulk}$. The Sr stratigraphy age model suggests we attain sample resolution for organic geochemistry between 10-20 kyr for the time interval of 22.5 to 23.1 Ma, and less than 40 kyr for the interval 24 to 23.1 Ma.

3.1.2 Site U1406

From IODP Site U1406, we used samples from Holes A, B, and C; due to heavy sampling on the splice (CCSF-A), some of the samples are off-splice with their depths mapped to the splice (CCSF-M), based on the composite depth scale and splice for that site(Van Peer et al., 2017). The record presented here spans an interval of roughly 30 m CCSF-M, which covers the time from 22.4 to 24 Ma. The sample resolution is ~10 kyr (with a 5 kyr standard deviation) on average between 22.4 and 23.0 Ma and increases to 20-60 kyr in the older section between 23.2 and 24 Ma. This spacing should enable a high-resolution record of SST changes during the Mi-1 deglaciation as well as an overall insight into the glaciation of the Mi-1 event. The ages for our samples were integrated from the published astronomically-tuned age model for the site from(Van Peer et al., 2024). To verify the off-splice sample stratigraphy, we generated $\delta^{18}O_{benthic}$ for an additional 10 samples.

3.2 Organic Geochemistry

Lipids (total lipid extract, TLE) were extracted from 25-35 g (Site U1406) and 30-40 g (Site 1168) of freeze-dried sediment using a Dionex 350 accelerated solvent extractor from Thermo. Three static cycles at 100°C with a dichloromethane to methanol (CH_2Cl_2/MeOH) ratio of 9:1 was used for the extraction process. An initial comparison of 14 samples from Site 1168 showed no difference in the chromatograms before and after saponification of the TLE with 0.5M KOH in 95:5 MeOH/H_2O, heated at 75°C for 2 hours. Therefore, the remaining samples were analyzed without saponification. For Site 1168, samples were processed with aluminium oxide columns using Hexane 9:1 DCM, Hexane 1:1 DCM, and DCM 1:1 MeOH. For Site U1406, standard elution of the TLE through silica gel columns was carried out as described previously(Guitián et al., 2019).

The ketone fraction which contains the alkenones was dried under a N_2 stream and dissolved in toluene for quantification at ETH Zürich using a Thermo Scientific Trace 1310 Gas Chromatograph (GC) equipped with a 105 m x 0.25 mm capillary column (Rtx-200, 0.25 µm film thickness, Restek) and a 5 m x 0.25 mm guard column (Agilent) with 1.5 ml/min He as carrier gas flow. Samples were injected into a programmable temperature vaporization (PTV) inlet and quantified by flame ionization detection (FID). GC oven held an initial temperature of 50°C from 2 minutes, ramped first by a temperature increase of 40°C/min to 250°C, then followed by 2.5°C/min to 300°C, and held isothermal for 35 minutes. Finally, it was ramped 10°C/min to 320°C and held for 5 minutes. For alkenone quantification, a known amount of an internal standard (*n*-alkanes) was added to the sample prior to injection. Additionally, an in-house alkenone standard with known concentration was regularly measured. The comparison of the peak areas of the sample with unknown alkenone concentration with the standards yielded sample alkenone concentration. The in-house alkenone standard measurement also served to identify instrument drift and ensure long-term validation.

The alkenone undersaturation index $U^{k'}_{37}$, a proxy for sea surface temperature (SST)(Prahl and Wakeham, 1987), was determined from the FID chromatogram by quantifying the relative abundance of the C_{37} di-unsaturated and tri-unsaturated alkenones. Alkenone-derived SST was calculated from $U^{k'}_{37}$ using the global core top calibration(Müller

https://doi.org/10.5194/egusphere-2026-3415
Preprint. Discussion started: 3 July 2026

et al., 1998). Where C_{38} methyl alkenones were sufficiently abundant for robust quantification, $U^{k'}_{38me}$ values were also determined and converted to SSTs estimate using the global core-top calibration from (Novak et al., 2022) which extends the upper temperature range of the proxy to approximately 32°C. At Site 1168, high alkenone abundance enabled reliable quantification of $U^{k'}_{38me,}$ whereas $U^{k'}_{37}$ measurements were occasionally affected by co-eluting compounds. Consequently, for subsequent temperature-dependent calculations for Site 1168, $U^{k'}_{38me}$ -derived SSTs were used where the $U^{k'}_{37}$ values were saturated or affected by co-eluting compounds, while the average of the $U^{k'}_{38me}$ and $U^{k'}_{37}$ temperature was used where both proxies yielded reliable results. In contrast, for Site U1406, only a limited number of samples contained sufficient alkenones for $U^{k'}_{38me}$ determination; we illustrate the $U^{k'}_{38me}$ for these samples for comparison, but discuss trends based on the more continuous $U^{k'}_{37}$ temperature record.

3.3 Carbonate stable isotope geochemistry

Carbon and oxygen isotopes of carbonate were measured as described previously for small carbonate samples on a GAS BENCH II system coupled to a Delta V Plus IRMS from Thermo Scientific at ETH Zürich. International (NBS-19 & 18) and in-house carbonate standards yielded a precision of 0.07‰(Breitenbach and Bernasconi, 2011). Values are reported relative to the VPDB standard.

3.3.1 Bulk carbonate

Bulk carbonate was measured for all samples from both sites and smear slides confirm that it consists dominantly of coccoliths of genera *Reticulofenestra*, as described in previous studies(Guitián et al., 2020).

For the $\delta^{18}O_{bulk}$ and $\delta^{13}C_{bulk}$ measurements, we used on average 150 µg of the freeze-dried sediment employed previously for organic extraction. Analyses were made using the GAS BENCH II system coupled to a Delta V Plus IRMS from Thermo Scientific, following the procedures described by(Breitenbach and Bernasconi, 2011). Analytical precision after the system was calibrated with two in-house standards was 0.07‰ for both stable isotopes. Values are reported relative to the VPDB standard.

3.3.2 Benthic foraminifera

For Site 1168 and a few intervals in Site U1406, we also analyzed stable isotopes on benthic foraminifera. For this, we used the sediment after organic extraction, since extraction does not alter isotopes or trace elements(Crumpton-Banks et al., 2022). Sediment was sieved in deionized water through a 150 µm sieve and oven dried overnight at 50°C. Where required due to high clay content, sediment was additionally sonicated and stirred in buffered water to disaggregate the foraminifera. Wherever possible, 5 specimens of genus *Cibicidoides* spp. mainly *Cibicidoides mundulus*, an epifaunal species which calcifies in oxygen isotopic equilibrium with ambient water (Bemis et al., 1998; Ravelo and Hillaire-Marcel, 2007) were picked from the >250 µm size fraction per sample. We also incorporate published analyses from the same core from (Guitián and Stoll, 2021) produced in the same laboratory with identical procedures.

For Site 1168, we also include digitized benthic isotope results on the *Cibicidoides mundulus* from(Pfuhl et al., 2004), which are adjusted by -0.5‰ (-0.64‰ and +0.14‰) to be compared to the values produced in this study. This adjustment removes a +0.64‰ species correction applied by(Pfuhl et al., 2004), since recent work by (Jöhnck et al., 2021) show that the epifaunal taxa *Cibicidoides mundulus* and *Cibicidoides wuellerstorfi* show no significant offset in $\delta^{18}O$ between water and calcite and only shallow infaunal *Cibicidoides* species exhibit higher variability. Additionally, we apply a +0.14‰ correction for the size fraction difference, because (Pfuhl et al., 2004) picked from the smaller >150µm size fraction. The size correction comes from (Barras et al., 2010) who describe a substantial

https://doi.org/10.5194/egusphere-2026-3415
Preprint. Discussion started: 3 July 2026

test size effect on $\delta^{18}O$ of benthic foraminifera (in their study, it is *Bulimina marginata* with an effect of 0.0014‰/μm) and we assume a similar effect for *Cibicidoides mundulus*.

3.4. Calculation of the local surface $\delta^{18}O_{sw}$

Variations in the $\delta^{18}O$ of seawater ($\delta^{18}O_{sw}$) in which the coccolithophores lived can be calculated using the temperature data from alkenone and $\delta^{18}O_{bulk}$. Across the OMT, there is no significant interspecies effect in isotopic values between small (<2.5 μm) and large (6-9 μm) coccoliths(Bolton and Stoll, 2013), which corresponds to the coccoliths' size range at Site 1168 and Site U1406 between 2.5 μm to 8 μm during the OMT(Guitián et al., 2020). Because the temperature dependence of coccolith $\delta^{18}O$ is indistinguishable from that of other biogenic carbonates(Hermoso et al., 2014), no additional knowledge of the intercept of the $\delta^{18}O_{coccolith}$-temperature equation for *Reticulofenestra* under late Oligocene to early Miocene conditions is needed to calculate relative changes in $\delta^{18}O_{sw}$, and we focus interpretations on the relative changes only. Absolute $\delta^{18}O_{sw}$ is uncertain because the magnitude of the constant vital effect applicable to the late Oligocene-early Miocene coccoliths is not well constrainted, and because the absolute temperatures reconstructed by $U^{k'}_{37}$ have been shown to significantly exceed calcification temperatures reconstructed by clumped isotopes in other Miocene mid-latitude sites(Mejía et al., 2025; Stoll et al., 2025). To reconstruct the variation in $\delta^{18}O_{sw}$, we employ the temperature dependence from (Hermoso et al., 2014) which is as follows:

$$\delta^{18}O_{sw} = \delta^{18}O_{bulk} - (0.0009 * T^2) + (0.2468 * T) - 3.7434 + 0.27 \quad (1)$$

To estimate the local component of surface $\delta^{18}O_{sw}$ which is distinct from the spatially averaged deep ocean $\delta^{18}O_{sw}$, we subtract $\delta^{18}O_{benthic}$ of Site U1406 (Van Peer et al., 2024) from our calculated surface $\delta^{18}O_{sw}$. For Site 1168, we subtract the surface $\delta^{18}O_{sw}$ from the $\delta^{18}O_{benthic}$ of the South Atlantic ODP Site 1264(Beddow et al., 2016). To minimize the effects of age uncertainty and capture signals >100 kyr frequency, we employ a smoothed $\delta^{18}O_{sw}$ and $\delta^{18}O_{benthic}$ (Fig. S1) and make the calculation only for the interval of high-resolution SST data between 22.5 and 24.8 Ma. Site 1264 is the coldest site in a global stack of benthic oxygen records over the OMT and has been proposed to be the most dominated by the ice volume changes(Beddow et al., 2016). If variations in $\delta^{18}O_{sw}$ at Site 1168 only records a common change in ice volume, and temperature variations in Site 1264's $\delta^{18}O_{benthic}$ are negligible, then the $\delta^{18}O_{sw} - \delta^{18}O_{benthic}$ of Site 1168 would be constant. Variations in the $\delta^{18}O_{sw} - \delta^{18}O_{benthic}$ can elucidate where surface water $\delta^{18}O_{sw}$ at the site has additional local/regional effects and/or when the deep ocean temperature contribution to Site 1264 $\delta^{18}O_{benthic}$ is variable. At Site U1406, for comparison with the $\delta^{18}O_{bulk,}$ the $\delta^{18}O_{benthic}$ at Site U1406 is used because it features no stratigraphic uncertainty relative to our samples; however, it is interpreted to contain a component of temperature variation(Van Peer et al., 2024).

4 Results

4.1 Age Models

Our proposed new age model for the OMT at Site 1168 is anchored by tuning the maximum $\delta^{18}O_{bulk}$ at 431.6 mbsf to the start of eccentricity cycle 57.2 at 23.05 Ma, marked by the most positive $\delta^{18}O_{benthic}$ value of 2.94‰. Compared to the mean $^{87}Sr/^{86}Sr$ age, the youngest five tie points move the assigned age from the median Sr age model by ~1 eccentricity cycle (younger), and the oldest three 3 tie points are between 1 and 1.5 eccentricity cycles older than the mean Sr age (Fig. S2). All of these shifts are within the uncertainty of the Sr ages, given that $^{87}Sr/^{86}Sr$ plateaus at the

https://doi.org/10.5194/egusphere-2026-3415
Preprint. Discussion started: 3 July 2026

OMT(Stoll et al., 2024). In the low resolution $\delta^{18}O_{benthic}$ data, heavy values are identified at 414 (and 416) mbsf, which are interpreted as Mi-1.1 (Billups, 2002) with an age of 22.58 Ma (eccentricity cycle 56.3). The sedimentation rate is roughly 50 m/Myr prior to the Mi-1 glaciation and decreases to 20 m/Myr after the deglaciation around 22 Ma. With the addition of tie points from the bulk carbonate records, the sedimentation rate strongly decreases from >60 m/Myr to <20 m/Myr during the Mi-1 glaciation, followed by an increase to >40 m/Myr during the deglaciation phase, suggesting a highly dynamic sedimentation regime over the OMT at this location (Fig. S2).

Our $\delta^{18}O_{bulk}$ record of Site U1406 is similar to the published high-resolution $\delta^{18}O_{benthic}$ record for same site, supporting the existing age model (Fig. 4). For the off-splice samples, our $\delta^{18}O_{benthic}$ record measurements from *Cibicidoides mundulus* are within the range of variation in the $\delta^{18}O_{benthic}$ record from the splice, although they suggest our sample selection has not captured the first $\delta^{18}O_{benthic}$ maximum at 23.25 Ma resolved by the high-resolution benthic record.

4.2 SST and Ocean Dynamics During the Mi-1 Glaciation

4.2.1 Site 1168

The sea surface temperatures (SSTs) recorded by $U^{k'}_{38me}$ at Site 1168 in the Tasmanian Margin decreases from 30.8 to 26.8°C between 23.9 to 22.2 Ma (Fig. 3a). The cooling occurs in two steps, each of ~2°C at 23.8 Ma and 23.4 Ma, although the first step may be underestimated due to initial $U^{k'}_{38}$ saturation. Our high-resolution sampling resolves significant 1-2°C orbital-scale temperature variability between 23.3 and 22.8 Ma. Within this variability, the mean SST warms by ~2°C. A third, more gradual cooling of 2°C occurs between ~22 and 21 Ma.

The $\delta^{18}O_{bulk}$ of Site 1168 gradually transitions to heavier values between 23.8 and 22.9 Ma, reaching several maxima between 23.2 and 22.9 Ma, and then recovers rapidly in several steps between 22.8 and 22.6 Ma (Fig. 3c). The new benthic *Cibicidoides* spp. $\delta^{18}O$ overall mirrors the $\delta^{18}O_{bulk}$ trend (apart from two samples around 22.6 Ma), but the increase in $\delta^{18}O_{benthic}$ between 23.8 and 22.7 Ma from 1 to almost 3‰ is almost twice as large as the changes observed in the $\delta^{18}O_{bulk}$.

The $\delta^{18}O_{sw}$ over the OMT in Site 1168 progressively decreases towards lighter values, punctuated by a temporary return to heavier values centered on 23.1 Ma (Fig. 3b). $\delta^{18}O_{sw}$ decreases by about 0.4‰ between the first cooling step at 23.8 and 23.6 Ma. There is a significant high frequency variation in the $\delta^{18}O_{sw}$ that ranges within 1.5‰. The evolution of $\delta^{18}O_{sw}$ differs significantly from both $\delta^{18}O_{bulk}$ and $\delta^{18}O_{benthic}$ during the Mi-1 and Mi-1.1 glaciation (22.58 Ma)(Billups et al., 2002), and the $\delta^{18}O_{sw} - \delta^{18}O_{benthic}$ indicates two transient periods of lower values during the Mi-1 and Mi-1.1 glaciation (Fig. 8)

https://doi.org/10.5194/egusphere-2026-3415
Preprint. Discussion started: 3 July 2026

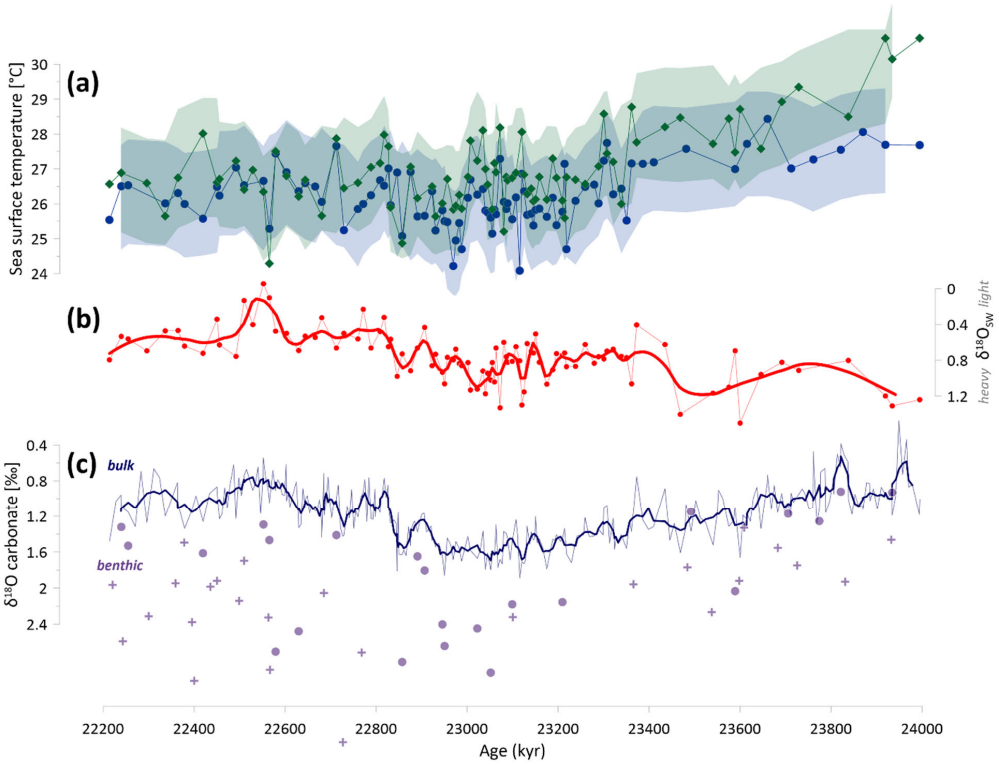

Figure 3. (a) Site 1168 SST estimated from $U^{k'}_{38me}$ (green diamonds) and $U^{k'}_{37}$ (blue circles), with the corresponding shaded regions representing the ±1.5°C uncertainty range smoothed with 3 point running mean. (b) Relative changes in surface $\delta^{18}O_{sw}$ calculated for Site 1168 where the values are referenced so that the lightest value around Mi-1.1 equals 0‰. (c) Bulk carbonate $\delta^{18}O$ with the thick blue line showing a ~25 kyr running average and the faint blue line indicating measured data. Circles represent new $\delta^{18}O_{benthic}$ data and crosses from(Pfuhl et al., 2004).

4.2.2 Site U1406

At Site U1406 in the Newfoundland margin, $U^{k'}_{37}$ SST records a mild cooling beginning at 23.7 Ma. However, there is an ~1°C increase in temperature beginning at 23.5 Ma before a more significant cooling of up to 3°C occurs at ~23.3 Ma (Fig. 4a). $U^{k'}_{38me}$ SSTs obtained for a few samples show a similar range as the $U^{k'}_{37}$ SST, with no evidence for higher temperatures in the $U^{k'}_{38me}$ SSTs despite its wider calibration range. Temperatures declined to about 25°C during the maximum glacial extent of the Mi-1 before gradually increasing by 2-3°C over the course of the following glacial-interglacial cycles. A second cold extreme at 22.58 Ma coincides with the Mi-1.1 glaciation, consistent with the positive $\delta^{18}O_{benthic}$ excursion.

Although the $\delta^{18}O_{bulk}$ measurements of Site U1406 sometimes exhibit high sample-to-sample variability, the long-term trend is similar to the $\delta^{18}O_{benthic}$ record from the same site (Fig. 4c). Both the initial ice growth phase on Antarctica between 23.8 and 23.6 Ma is reflected as a ~0.8‰ increase and the distinct eccentricity-paced cycles between 23 and 22.5 Ma can be clearly identified. The local $\delta^{18}O_{sw}$ mimics the same trend described by the $\delta^{18}O_{benthic}$ record during the Mi-1 glaciation with an initial change of ~0.6‰ between 23.8 and 23.6 Ma, followed by a partial recovery towards 23.3 Ma (Fig. 4b). The $\delta^{18}O_{sw} - \delta^{18}O_{benthic}$ is lower between 23.0 to 23.2 Ma and at 22.5 Ma (Fig. 8).

https://doi.org/10.5194/egusphere-2026-3415
Preprint. Discussion started: 3 July 2026

In the interval following the OMT, from 23 to 22.4 Ma, our high sample density resolves high frequency variations in the local $\delta^{18}O_{sw}$ in the order of 0.4‰. Potentially these cycles are paced by obliquity with additional amplitude modulation during high eccentricity, but in our record and sampling resolution neither obliquity nor eccentricity are detected as significant by spectral analysis.

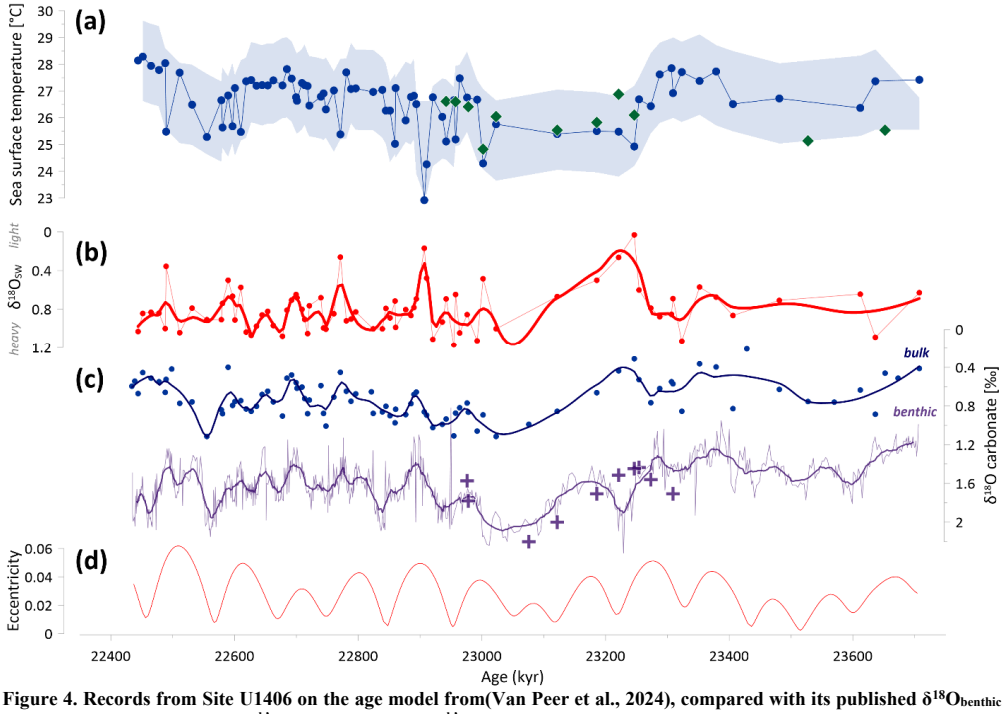

Figure 4. Records from Site U1406 on the age model from(Van Peer et al., 2024), compared with its published $\delta^{18}O_{benthic}$ record. (a) SST derived from $U^{k'}_{37}$ (blue circles) and $U^{k'}_{38me}$ (green diamonds), with shaded region representing the ±1.5°C uncertainty range of the $U^{k'}_{37}$ SST. (b) Relative variation in local $\delta^{18}O_{sw}$, with the lightest value referenced to 0‰. (c) Top curve represents $\delta^{18}O_{bulk}$ from fine fraction carbonate and bottom curve is $\delta^{18}O_{benthic}$ record from (Van Peer et al., 2024) with a 41-kyr moving average. The plus symbols represent $\delta^{18}O_{benthic}$ of samples from this study. (d) Eccentricity from(Laskar et al., 2004). $\delta^{18}O_{sw}$ and $\delta^{18}O_{bulk}$ presented with a quadratic gaussian LOESS moving average with a span of 0.1.

5 Discussion

5.1 Surface ocean conditions across the OMT in the Newfoundland Margin versus the Tasman Margin

Our SST record from Site 1168 in the Tasmanian Margin, similar to the $\delta^{18}O_{benthic}$ trend, shows that the cooling during the OMT glaciation occurs in two steps, each of at least ~2°C centered at 23.8 and 23.3 Ma during the Mi-1 glaciation (Fig. 3). This new record confirms the onset of surface ocean cooling in the Southern Hemisphere mid-latitudes by 23.8 Ma and its subsequent intensification starting around 23.3 Ma; this is coincident within age model uncertainty with the positive $\delta^{18}O_{benthic}$ shift interpreted as the two-step AIS expansion(Liebrand et al., 2017). Site U1356 located in the Wilkes Land continental margin in Antarctica also shows an extreme surface cooling of 8 to 12°C during this interval(Hartman et al., 2018), interpreted as consequence of deep marine connection in the Drake Passage(Hoem et al., 2023).

Temperatures in the Newfoundland site exhibit similar trends to the Southern Ocean during most of the intervals of our record (Fig. 5). Our high-resolution SST at Site U1406 in the Newfoundland Margin, which begins at 23.7 Ma, does not sample the first large cooling step recorded at Site 1168. However, synchronous with the start of the second

https://doi.org/10.5194/egusphere-2026-3415
Preprint. Discussion started: 3 July 2026

cooling step at Site 1168, Site U1406 instead shows a 1°C warming between 23.5 and 23.3 Ma, a trend that contrasts with the positive shift in the $\delta^{18}O_{benthic}$ at Site U1406 during the Mi-1 glaciation (Fig. 5). Thereafter the abrupt nearly 3°C cooling at Site U1406 at 23.3 Ma is synchronous with the continued cooling at Site 1168 and both attain a period of sustained minimum temperatures until 22.9 Ma. Following the OMT, the average temperatures warm in both sites coincident with the trend to lighter $\delta^{18}O_{benthic}$, and with a greater magnitude of warming in Site U1406. This interval is marked by high amplitude orbital scale variability in both hemispheres.

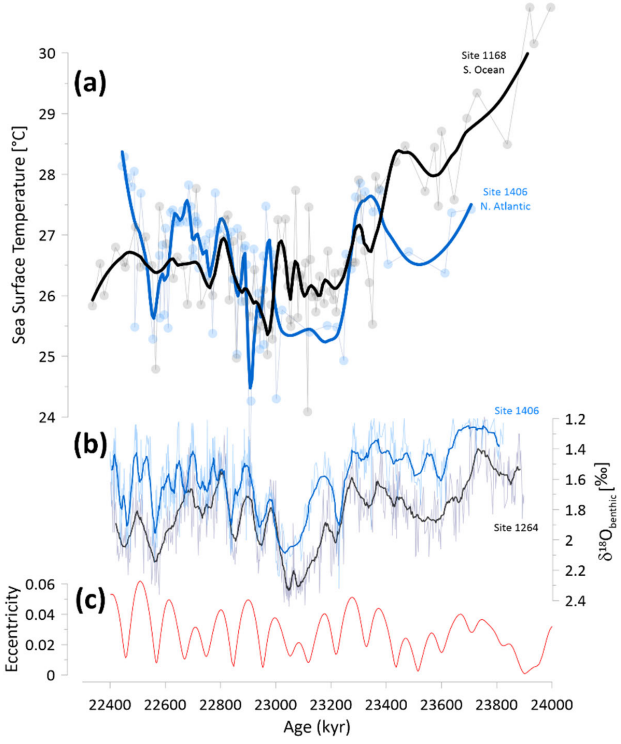

Figure 5. Variation in (a) SST in the North Atlantic Site U1406 compared to the Southern Ocean Site 1168, referenced to (b) $\delta^{18}O_{benthic}$ from Site U1406 (Van Peer et al., 2024) and Site 1264 (Liebrand et al., 2017) and (c) eccentricity(Laskar et al., 2004).

https://doi.org/10.5194/egusphere-2026-3415
Preprint. Discussion started: 3 July 2026

Although records from only two locations are too limited to infer global trends and processes, intervals with similar temperature evolution could be consistent with global climate forcing such as greenhouse gases or major changes in albedo due to changes in areas of snow and ice cover. Intervals of anti-phase temperature change, as observed from 23.5 to 23.3 Ma between the two records, may reflect changes in ocean heat transport, a mechanism previously invoked to explain intervals of anti-phase SST trends between the northwest North Atlantic Ocean and the subantarctic South Atlantic Ocean during the Eocene-Oligocene Termination (EOT)(Liu et al., 2018).

Following the Mi-1 glaciation, greenhouse gas feedback has been proposed to be a mechanism consistent with a global temperature recovery. Methane (CH_4) has been proposed to provide greenhouse gas forcing of deglaciations when glacial sea level lowstands lead to destabilization of methane hydrates and the release of methane to the atmosphere(Kim and Zhang, 2022). Periods of methane hydrate release have been inferred from lipid biomarkers attributed to archeal methanotrophy. On our revised age model, periods of elevated methanotrophic biomarkers at Site 1168 (Kim and Zhang, 2022) coincides with the sea level lowstand of the early Miocene Mi-1.1 glaciation (Fig. 6), potentially consistent with the proposed methane hydrate dissociation at this event. However, on the revised age model, the published lipid biomarker data does not span the Mi-1 period of AIS expansion and lowstand, so the importance of methane release in the deglaciation from MI-1 requires further assessment in future work (Fig. 6).

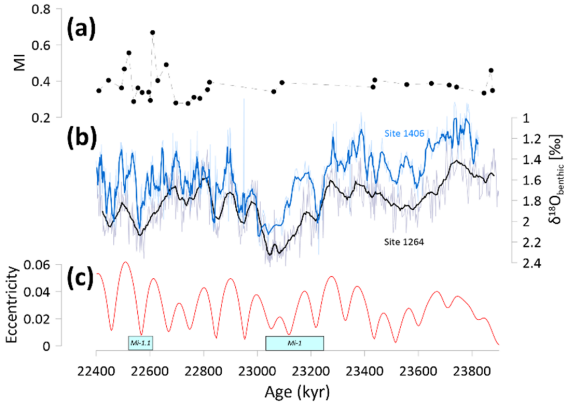

Figure 6. (a) MI index showing the presence of lipid biomarkers attributed to archeal methanotrophy(Kim and Zhang, 2022). (b) $\delta^{18}O_{benthic}$ records from Site U1406 (Van Peer et al., 2024) and Site 1264 (Liebrand et al., 2017) and (c) eccentricity(Laskar et al., 2004). Blue boxes indicate the Mi-1 and Mi-1.1 glaciations.

5.2 Amplified intermediate water cooling in the Southern Ocean

Between 24 to 23 Ma, ODP Site 1168 exhibits a much higher amplitude change in $\delta^{18}O_{benthic}$ (~2‰) at ~1000 m water depth compared to deeper South Atlantic (ODP Site 1264 at 2000 m, 1‰; ODP Site 1090 at >3000 m, 1.4‰) or deeper (3000-4000 m) tropical Atlantic (Sites 926, 929) or Pacific (ODP Sites 1218, U1334) sites (Fig. 7). We attribute this larger amplitude change to greater intermediate water cooling at the Tasman Rise compared to the deep ocean.

Prior to the onset of the Mi-1 glaciation, the waters bathing Site 1168 feature $\delta^{18}O_{benthic}$ intermediate between that of deep Atlantic tropical Sites 926 and 929 and deep Southern Ocean Sites 1264 and 1090. By the OMT, the intermediate waters at Site 1168 feature the most positive $\delta^{18}O_{benthic}$ and thus indicative of coldest and/or most saline waters of all these sites (Fig. 7). The magnitude of the $\delta^{18}O_{benthic}$ change at Site 1168 significantly exceeds the magnitude attributed to the ice volume effect in other deep-sea sites(Beddow et al., 2016; Liebrand et al., 2017). At 0.22‰ per 1°C of cooling(Kim and O'neil, 1997), the intermediate water record suggests up to 4°C more cooling of intermediate waters compared to South Atlantic deep waters.

https://doi.org/10.5194/egusphere-2026-3415
Preprint. Discussion started: 3 July 2026

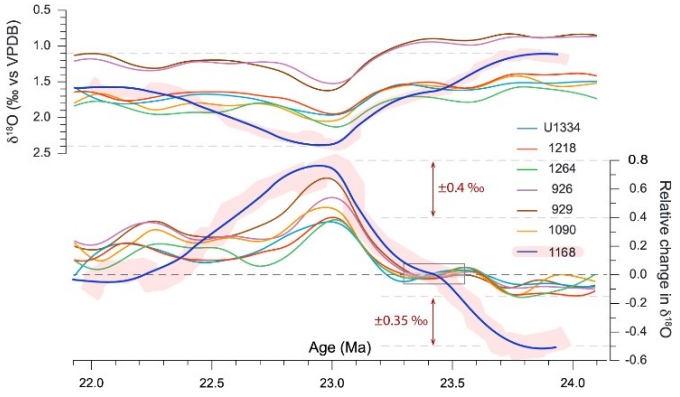

Figure 7. Statistically smoothed $\delta^{18}O_{benthic}$ data sets from Sites U1334, 1218, 1264, 926, 929 and 1090 as presented by (Beddow et al., 2016) with the smoothed Site 1168 record. Relative change in $\delta^{18}O$ uses a baseline average determined between 23.3 and 23.5 Ma, indicated by the grey shaded box. (Lower resolution) data from this study is overprinted (blue), which is produced using a 10% LOWESS smooth (instead of the SiZer smooths for the other sites).

Strong cooling at the Antarctic margin is consistent with amplified intermediate water cooling in the Southern Ocean. In the Late Oligocene, the temperature gradient across the Australian-Antarctic Gulf between Site 1168 and Site U1356 (offshore Wilkes Land) increased from 6°C prior to 26 Ma to more than 9°C at the start of the Mi-1 glaciation around 24 Ma(Hoem et al., 2022). Amplified cooling of intermediate waters in the Southern Ocean implies significant temperature change in high latitude regions where such waters outcrop. The high frequency 1 to 1.5 ‰ variation in $\delta^{18}O_{benthic}$ at Site 1168 implies that intermediate water temperatures oscillated significantly both at the onset of ice buildup as well as during the OMT and in the early Miocene. Sea ice extent and duration may be one process contributing to the rapid, high amplitude variation in circum-Antarctic and intermediate water temperatures.

5.3 Variations in local $\delta^{18}O_{sw}$

Surface waters at Site 1168 at the Tasman Rise experienced a long-term decrease in $\delta^{18}O_{sw}$ between 23.8 and 22.5 Ma. We suggest that reduced import of saline waters by the Leeuwin Current may have contributed to the long-term decrease in $\delta^{18}O_{sw}$ at the site. While there is a steep (0.7‰) surface ocean $\delta^{18}O_{sw}$ gradient across the modern Australian-Antarctic Gulf, with significantly fresher waters south of the Subtropical front(Legrande and Schmidt, 2006), and dinoflagellate assemblages indicate that the subpolar region at paleolatitude 60°S off the Wilkes Land margin (Evangelinos et al., 2020) experienced periodic equatorward frontal movement in the latest Oligocene-earliest Miocene, the dinocyst biogeography at Site 1168 indicates that site was situated continuously north of the frontal systems during this time (Hou et al., 2023) with a stable abundance of north-of-the-subtropical front species(Thöle et al., 2023). Additionally, coupled ocean-atmosphere GCM simulations (Bradshaw et al., 2021) suggest very limited changes in salinity (<0.5 psu) at this site over a broad range of pCO_2 or Antarctic ice sheet area or volume; if the modern salinity ^{18}O slope of 0.43‰/psu were applicable to the surface ocean at this time, it would entail a <0.2‰ change in the $\delta^{18}O_{sw}$. If the model representation of frontal response to broad scale climate is accurate, the model and dinocyst results both suggest that changes in frontal position alone were unlikely to have caused the long-term freshening trend and the two periods of more pronounced freshening during Mi-1 and Mi-1.1 ice expansion. At the same time, the low abundance of terrestrial palynomorphs and terrestrial amorphous organic matter in Site 1168 (Hoem et al., 2021b; Brinkhuis et al., 2003; Hou et al., 2023) suggests that the site was not proximal to the outflow of major river systems and therefore unlikely to be influenced by low salinity river plumes. This suggests changes in salt transport from the subtropical gyre via the Leeuwin Current as a likely mechanism for variable local freshening.

While not experiencing a significant long-term trend, the surface ocean $\delta^{18}O_{sw}$ at Site U1406 in the North Atlantic nevertheless fluctuated significantly across the OMT. Over the latest Oligocene, the site shows more saline conditions during warmer SST (Fig. 4; Fig S3), which is the opposite expectation for the response of high latitude (and deep ocean) temperature and global ice volume based on middle Oligocene paired benthic $\delta^{18}O$ and Mg/Ca(Brzelinski et al., 2023). Potentially, the trend in local surface $\delta^{18}O_{sw}$ at this site reflects not only a component due to Antarctic ice volume but also variations in salinity due to changing Gulf Stream, a process consistent with the positive correlation between $\delta^{18}O_{sw}$ and SST given the influence of the Gulf Stream on both heat and salt in this setting (Fig. 2). In the Middle Oligocene, variations in the Northern Atlantic gyre

https://doi.org/10.5194/egusphere-2026-3415
Preprint. Discussion started: 3 July 2026

dynamics at Site U1406 have contributed significant high and low frequency alterations in the $\delta^{18}O_{sw}$ of the upper ocean, calculated from sub-thermocline foraminifera when removing the bottom water ice-volume $\delta^{18}O_{sw}$ signal(Brzelinski et al., 2023). Thus, both regional current dynamics and global ice volume may influence the local surface water $\delta^{18}O_{sw}$ at Site U1406. Both Site U1406 and 1168 show negative anomalies in $\delta^{18}O_{sw} - \delta^{18}O_{benthic}$ during the cooling phases of Mi-1 and that of Mi-1.1. If the $\delta^{18}O_{benthic}$ were responding only to ice volume with a comparable magnitude $\delta^{18}O_{sw}$ change in the surface and deep oceans, the $\delta^{18}O_{sw} - \delta^{18}O_{benthic}$ would be constant. However, the negative shift in the $\delta^{18}O_{sw} - \delta^{18}O_{benthic}$ could be explained by significant deep ocean cooling at both Site U1406 and Site 1264 (used as the reference for Site 1168), during the Mi-1 and Mi-1.1 events.

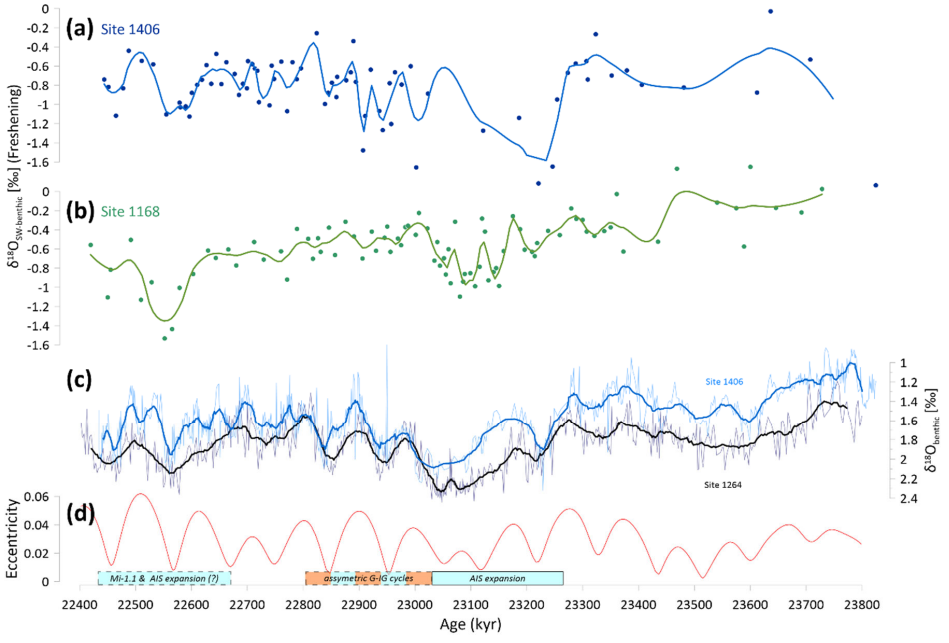

Figure 8. Relative local surface water freshening calculated as $\delta^{18}O_{sw} - \delta^{18}O_{benthic}$ for (a) Site U1406 and (b) Site 1168, with the heaviest values for each site anchored to 0‰. c) $\delta^{18}O_{benthic}$ for Site U1406 (Van Peer et al., 2024) and Site 1264 (Liebrand et al., 2017) with a ~50-kyr moving average. (e) Eccentricity (Laskar et al., 2004). The vertical blue shaded bars highlight glacial periods identified with heavy $\delta^{18}O_{bulk}$ that occur with low SST and εp. Because of how the age model is constructed, heavy $\delta^{18}O_{bulk}$ align with heavy $\delta^{18}O_{benthic}$.

6 Conclusions

New alkenone-based SST estimates from the Newfoundland Margin and the Tasmanian Rise spanning the OMT confirm that both sites experienced cooling over the 0.5 to 1 m.y. period preceding the benthic $\delta^{18}O$ maximum which has been interpreted to reflect a major Antarctic Ice Sheet expansion at the Mi-1. The longer record from Site 1168 on the Tasman Rise resolves the cooling in two steps, each about 2°C. At the 10^5 to 10^6 yr timescale resolved by our sampling density, bulk carbonate $\delta^{18}O$ at Site 1406 and Site 1168 exhibit similar timing and magnitude changes as deep ocean benthic $\delta^{18}O$ records from the North Atlantic (Site 1406) and South Atlantic (Site 1264) basins, respectively. Although the resolution of published and our new benthic $\delta^{18}O$ record from Site 1168 does not capture astronomical variability, its higher amplitude $\delta^{18}O$ change across the OMT suggests that the intermediate waters bathing Site 1168 experienced a higher amplitude of temperature change across the OMT than most deep basin sites. While benthic $\delta^{18}O$ suggests a transient anomaly over the Mi-1 glaciation with recovery by 22.9 Ma of values comparable to those at 23.3 Ma, the SST record of Site 1168 suggests a larger magnitude of pre-OMT cooling and limited recovery of SST after the benthic $\delta^{18}O$ maximum. This suggests that for the southern high mid-latitudes, the OMT reflects a step change rather than transient climate event.

https://doi.org/10.5194/egusphere-2026-3415
Preprint. Discussion started: 3 July 2026

Author contributions

The study was conceived by HS and the doctoral thesis of TT was supervised by HS and IHA. TT and MS completed the biomarker preparation and analysis, supported by RW. PB contributed interpretation on Site 1168. TvP contributed sampling strategy, age model development and interpretation from Site U1406. The manuscript was written by H.S. and A.M. based on thesis chapters by T.T.

Acknowledgments

Sediment samples were provided by the Integrated Ocean Drilling Program (IODP). We thank Madalina Jaggi, Stewart Bishop, and Thierry Solms from Climate Geology Group at ETH Zurich for their support and assistance in the laboratory. This research was funded by the Swiss National Science Foundation (Awards 200021_182070 and grant no. 200021L-227444 to Heather Stoll).

Data availability

The data tables will be available in the ETH Research Collection under the following link: https://doi.org/10.3929/ethz-c-000801115. The embargo on access will be removed upon acceptance of the article.

https://doi.org/10.5194/egusphere-2026-3415
Preprint. Discussion started: 3 July 2026

References

Barras, C., Duplessy, J.-C., Geslin, E., Michel, E., and Jorissen, F.: Calibration of δ 18 O of cultured benthic foraminiferal calcite as a function of temperature, Biogeosciences, 7, 1349-1356, 2010.

Beddow, H. M., Liebrand, D., Sluijs, A., Wade, B. S., and Lourens, L. J.: Global change across the Oligocene-Miocene transition: High-resolution stable isotope records from IODP Site U1334 (equatorial Pacific Ocean), Paleoceanography, 31, 81-97, 2016.

Bemis, B. E., Spero, H. J., Bijma, J., and Lea, D. W.: Reevaluation of the oxygen isotopic composition of planktonic foraminifera: Experimental results and revised paleotemperature equations, Paleoceanography, 13, 150-160, 1998.

Billups, K.: Late Miocene through early Pliocene deep water circulation and climate change viewed from the sub-Antarctic South Atlantic, Palaeogeography, Palaeoclimatology, Palaeoecology, 185, 287-307, 2002.

Billups, K., Channell, J., and Zachos, J.: Late Oligocene to early Miocene geochronology and paleoceanography from the subantarctic South Atlantic, Paleoceanography, 17, 4-1-4-11, 2002.

Blaauw, M. and Christen, J. A.: Flexible paleoclimate age-depth models using an autoregressive gamma process, 2011.

Bolton, C. T. and Stoll, H. M.: Late Miocene threshold response of marine algae to carbon dioxide limitation, Nature, 500, 558-562, 2013.

Boyle, P. R., Romans, B. W., Tucholke, B. E., Norris, R. D., Swift, S. A., and Sexton, P. F.: Cenozoic North Atlantic deep circulation history recorded in contourite drifts, offshore Newfoundland, Canada, Marine Geology, 385, 185-203, doi.org/10.1016/j.margeo.2016.12.014, 2017.

Bradshaw, C. D., Langebroek, P. M., Lear, C. H., Lunt, D. J., Coxall, H. K., Sosdian, S. M., and de Boer, A. M.: Hydrological impact of Middle Miocene Antarctic ice-free areas coupled to deep ocean temperatures, Nature Geoscience, 14, 429-436, 2021.

Breitenbach, S. F. and Bernasconi, S. M.: Carbon and oxygen isotope analysis of small carbonate samples (20 to 100 µg) with a GasBench II preparation device, Rapid Communications in Mass Spectrometry, 25, 1910-1914, 2011.

Brinkhuis, H., Munsterman, D., Sengers, S., Sluijs, A., Warnaar, J., and Williams, G.: Late Eocene to Quaternary dinoflagellate cysts from ODP Site 1168, off western Tasmania, Proceedings of the Ocean Drilling Program. Scientific Results,

Brzelinski, S., Bornemann, A., Liebrand, D., van Peer, T. E., Wilson, P. A., and Friedrich, O.: Large obliquity-paced Antarctic ice-volume fluctuations suggest melting by atmospheric and ocean warming during late Oligocene, Communications Earth & Environment, 4, 222, 2023.

Cande, S. C. and Stock, J. M.: Pacific—Antarctic—Australia motion and the formation of the Macquarie Plate, Geophysical Journal International, 157, 399-414, 2004.

Coxall, H. K., Wilson, P. A., Pälike, H., Lear, C. H., and Backman, J.: Rapid stepwise onset of Antarctic glaciation and deeper calcite compensation in the Pacific Ocean, Nature, 433, 53-57, 2005.

Crumpton-Banks, J. G., Tanner, T., Hernández Almeida, I., Rae, J. W., and Stoll, H.: No impact of alkenone extraction on foraminiferal stable isotope, trace element and boron isotope geochemistry, Biogeosciences, 19, 5633-5644, 2022.

Egger, L. M., Bahr, A., Friedrich, O., Wilson, P. A., Norris, R. D., Van Peer, T. E., Lippert, P. C., Liebrand, D., and Pross, J.: Sea-level and surface-water change in the western North Atlantic across the Oligocene–Miocene Transition: a palynological perspective from IODP Site U1406 (Newfoundland margin), Marine Micropaleontology, 139, 57-71, doi.org/10.1016/j.marmicro.2017.11.003, 2018.

Evangelinos, D., Escutia, C., Etourneau, J., Hoem, F., Bijl, P., Boterblom, W., van de Flierdt, T., Valero, L., Flores, J.-A., and Rodriguez-Tovar, F. J.: Late oligocene-miocene proto-antarctic circumpolar current dynamics off the Wilkes Land margin, East Antarctica, Global and Planetary Change, 191, 103221, 2020.

Evans, D., Brugger, J., Inglis, G. N., and Valdes, P.: The temperature of the deep ocean is a robust proxy for global mean surface temperature during the Cenozoic, Paleoceanography and Paleoclimatology, 39, e2023PA004788, 2024.

Exon, N. F., Kennett, J. P., Malone, M. J., Brinkhuis, H., Chaproniere, G. C., Ennyu, A., and Shevenell, A. E.: The Tasmanian Gateway: Cenozoic climatic and oceanographic development, 2001.

Fuller, M. and Touchard, Y.: On the magnetostratigraphy of the East Tasman Plateau Timing of the opening of the Tasmanian Gateway and paleoenvironmental changes, Geophysical Monograph Series, 151, 63-78, 2004.

Goldner, A., Herold, N., and Huber, M.: Antarctic glaciation caused ocean circulation changes at the Eocene–Oligocene transition, Nature, 511, 574-577, 2014.

Guitián, J. and Stoll, H. M.: Evolution of Sea Surface Temperature in the Southern Mid-latitudes from Late Oligocene through Early Miocene, Paleoceanography and Paleoclimatology, 36, e2020PA004199, doi.org/10.1029/2020PA004199, 2021.

Guitián, J., Dunkley Jones, T., Hernández-Almeida, I., Löffel, T., and Stoll, H. M.: Adaptations of coccolithophore size to selective pressures during the Oligocene to Early Miocene high CO2 world, Paleoceanography and Paleoclimatology, 35, e2020PA003918, 2020.

Guitián, J., Phelps, S., Polissar, P. J., Ausín, B., Eglinton, T. I., and Stoll, H. M.: Midlatitude Temperature Variations in the Oligocene to Early Miocene, Paleoceanography and Paleoclimatology, 34, 1328-1343, 2019.

https://doi.org/10.5194/egusphere-2026-3415
Preprint. Discussion started: 3 July 2026

Hartman, J. D., Sangiorgi, F., Salabarnada, A., Peterse, F., Houben, A. J., Schouten, S., Brinkhuis, H., Escutia, C., and Bijl, P. K.: Paleoceanography and ice sheet variability offshore Wilkes Land, Antarctica–Part 3: Insights from Oligocene–Miocene TEX 86-based sea surface temperature reconstructions, Climate of the Past, 14, 1275-1297, 2018.

Hermoso, M., Horner, T. J., Minoletti, F., and Rickaby, R. E.: Constraints on the vital effect in coccolithophore and dinoflagellate calcite by oxygen isotopic modification of seawater, Geochimica et cosmochimica acta, 141, 612-627, 2014.

Hochmuth, K., Gohl, K., Leitchenkov, G., Sauermilch, I., Whittaker, J. M., Uenzelmann-Neben, G., Davy, B., and De Santis, L.: The evolving paleobathymetry of the circum-Antarctic Southern Ocean since 34 Ma: A key to understanding past cryosphere-ocean developments, Geochemistry, Geophysics, Geosystems, 21, e2020GC009122, 2020.

Hoem, F. S., Sauermilch, I., Hou, S., Brinkhuis, H., Sangiorgi, F., and Bijl, P. K.: Late Eocene–early Miocene evolution of the southern Australian subtropical front: a marine palynological approach, Journal of Micropalaeontology, 40, 175-193, 2021b.

Hoem, F. S., Sauermilch, I., Aleksinski, A. K., Huber, M., Peterse, F., Sangiorgi, F., and Bijl, P. K.: Strength and variability of the Oligocene Southern Ocean surface temperature gradient, Communications Earth & Environment, 3, 322, doi.org/10.1038/s43247-022-00666-5, 2022.

Hoem, F. S., Valero, L., Evangelinos, D., Escutia, C., Duncan, B., McKay, R. M., Brinkhuis, H., Sangiorgi, F., and Bijl, P. K.: Temperate Oligocene surface ocean conditions offshore of Cape Adare, Ross Sea, Antarctica, Climate of the Past, 17, 1423-1442, 2021a.

Hoem, F. S., López-Quirós, A., Van De Lagemaat, S., Etourneau, J., Sicre, M.-A., Escutia, C., Brinkhuis, H., Peterse, F., Sangiorgi, F., and Bijl, P. K.: Late Cenozoic sea-surface-temperature evolution of the South Atlantic Ocean, Climate of the Past, 19, 1931-1949, 2023.

Hou, S., Lamprou, F., Hoem, F. S., Hadju, M. R. N., Sangiorgi, F., Peterse, F., and Bijl, P. K.: Lipid biomarker-based sea (sub) surface temperature record offshore Tasmania over the last 23 million years, Climate of the Past Discussions, 2022, 1-33, 2022.

Hou, S., Stap, L. B., Paul, R., Nelissen, M., Hoem, F. S., Ziegler, M., Sluijs, A., Sangiorgi, F., and Bijl, P. K.: Reconciling Southern Ocean fronts equatorward migration with minor Antarctic ice volume change during Miocene cooling, Nature Communications, 14, 7230, 2023.

Jöhnck, J., Holbourn, A., Kuhnt, W., and Andersen, N.: Oxygen isotope offsets in deep-water benthic foraminifera, Journal of Foraminiferal Research, 51, 225-244, 2021.

Kim, B. and Zhang, Y. G.: Methane hydrate dissociation across the Oligocene–Miocene boundary, Nature Geoscience, 15, 203-209, doi.org/10.1038/s41561-022-00895-5, 2022.

Kim, S.-T. and O'Neil, J. R.: Equilibrium and nonequilibrium oxygen isotope effects in synthetic carbonates, Geochimica et cosmochimica acta, 61, 3461-3475, 1997.

Laskar, J., Robutel, P., Joutel, F., Gastineau, M., Correia, A., and Levrard, B.: A long-term numerical solution for the insolation quantities of the Earth, Astronomy & Astrophysics, 428, 261-285, 2004.

LeGrande, A. N. and Schmidt, G. A.: Global gridded data set of the oxygen isotopic composition in seawater, Geophysical research letters, 33, 2006.

Levy, R. H., Meyers, S., Naish, T. R., Golledge, N. R., McKay, R. M., Crampton, J. S., DeConto, R., De Santis, L., Florindo, F., and Gasson, E. G.: Antarctic ice-sheet sensitivity to obliquity forcing enhanced through ocean connections, Nature Geoscience, 12, 132-137, 2019.

Liebrand, D., Beddow, H. M., Lourens, L. J., Pälike, H., Raffi, I., Bohaty, S. M., Hilgen, F. J., Saes, M. J., Wilson, P. A., and van Dijk, A. E.: Cyclostratigraphy and eccentricity tuning of the early Oligocene through early Miocene (30.1–17.1 Ma): Cibicides mundulus stable oxygen and carbon isotope records from Walvis Ridge Site 1264, Earth and Planetary Science Letters, 450, 392-405, doi.org/10.1016/j.epsl.2016.06.007, 2016.

Liebrand, D., de Bakker, A. T. M., Beddow, H. M., Wilson, P. A., Bohaty, S. M., Ruessink, G., Palike, H., Batenburg, S. J., Hilgen, F. J., Hodell, D. A., Huck, C. E., Kroon, D., Raffi, I., Saes, M. J. M., van Dijk, A. E., and Lourens, L. J.: Evolution of the early Antarctic ice ages, Proc Natl Acad Sci U S A, 114, 3867-3872, 2017.

Liu, Z., He, Y., Jiang, Y., Wang, H., Liu, W., Bohaty, S. M., and Wilson, P. A.: Transient temperature asymmetry between hemispheres in the Palaeogene Atlantic Ocean, Nature Geoscience, 11, 656-660, doi.org/10.1038/s41561-018-0182-9, 2018.

Lunt, D. J., Valdes, P. J., Jones, T. D., Ridgwell, A., Haywood, A. M., Schmidt, D. N., Marsh, R., and Maslin, M.: CO2-driven ocean circulation changes as an amplifier of Paleocene-Eocene thermal maximum hydrate destabilization, Geology, 38, 875-878, 2010.

Mejía, L. M., Bernasconi, S. M., Fernandez, A., Zhang, H., Guitián, J., Jaggi, M., Taylor, V. E., Perez-Huerta, A., and Stoll, H.: Coccolith clumped isotopes reveal modest rather than extreme northern high latitude amplification during the Miocene, Nature Communications, 16, 10981, 2025.

Miller, K. G., Feigenson, M. D., Wright, J. D., and Clement, B. M.: Miocene isotope reference section, Deep Sea Drilling Project Site 608: an evaluation of isotope and biostratigraphic resolution, Paleoceanography, 6, 33-52, doi.org/10.1029/90PA01941, 1991.

Müller, P. J., Kirst, G., Ruhland, G., Von Storch, I., and Rosell-Melé, A.: Calibration of the alkenone paleotemperature index U37K′ based on core-tops from the eastern South Atlantic and the global ocean (60 N-60 S), Geochimica et cosmochimica Acta, 62, 1757-1772, 1998.

https://doi.org/10.5194/egusphere-2026-3415
Preprint. Discussion started: 3 July 2026

Naish, T. R., Duncan, B., Levy, R., McKay, R. M., Escutia, C., De Santis, L., Colleoni, F., Gasson, E. G., DeConto, R. M., and Wilson, G.: Antarctic Ice Sheet dynamics during the Late Oligocene and Early Miocene: climatic conundrums revisited, in: Antarctic Climate Evolution, Elsevier, 363-387, 2022.

Norris, R., Wilson, P., and Blum, P.: Proceedings of the Integrated Ocean Drilling Program Exp. 342, College Station, TX: Integrated Ocean Drilling Program, doi.org/10.2204/iodp.proc.342.107.2014, 2014.

Novak, J., McGrath, S. M., Wang, K. J., Liao, S., Clemens, S. C., Kuhnt, W., and Huang, Y.: U38MEK′ Expands the linear dynamic range of the alkenone sea surface temperature proxy, Geochimica et Cosmochimica Acta, 328, 207-220, 2022.

Pälike, H., Norris, R. D., Herrle, J. O., Wilson, P. A., Coxall, H. K., Lear, C. H., Shackleton, N. J., Tripati, A. K., and Wade, B. S.: The heartbeat of the Oligocene climate system, science, 314, 1894-1898, DOI: 10.1126/science.1133822, 2006.

Pfuhl, H. A. and McCave, I. N.: Integrated age models for the early Oligocene-early Miocene, sites 1168 and 1170–1172, Proc. ODP, Sci. Results, 1-21,

Pfuhl, H. A., Mccave, I. N., Schellenberg, S. A., and Ferretti, P.: Changes in Southern Ocean circulation in late Oligocene to early Miocene time, The Cenozoic Southern Ocean: Tectonics, Sedimentation, and Climate Change Between Australia and Antarctica, 151, 173-189, 2004.

Prahl, F. G. and Wakeham, S. G.: Calibration of unsaturation patterns in long-chain ketone compositions for palaeotemperature assessment, Nature, 330, 367-369, 1987.

Ravelo, A. C. and Hillaire-Marcel, C.: Chapter eighteen the use of oxygen and carbon isotopes of foraminifera in paleoceanography, Developments in marine geology, 1, 735-764, 2007.

Salabarnada, A., Escutia, C., Röhl, U., Nelson, C. H., McKay, R., Jiménez-Espejo, F. J., Bijl, P. K., Hartman, J. D., Strother, S. L., and Salzmann, U.: Paleoceanography and ice sheet variability offshore Wilkes Land, Antarctica–Part 1: Insights from late Oligocene astronomically paced contourite sedimentation, Climate of the Past, 14, 991-1014, 2018.

Scher, H. D., Whittaker, J. M., Williams, S. E., Latimer, J. C., Kordesch, W. E., and Delaney, M. L.: Onset of Antarctic Circumpolar Current 30 million years ago as Tasmanian Gateway aligned with westerlies, Nature, 523, 580-583, doi.org/10.1038/nature14598, 2015.

Schlitzer, R.: Ocean Data View., http://odv.awi.de, 2017.

Śliwińska, K. K., Dybkjær, K., Schoon, P. L., Beyer, C., King, C., Schouten, S., and Nielsen, O. B.: Paleoclimatic and paleoenvironmental records of the Oligocene–Miocene transition, central Jylland, Denmark, Marine Geology, 350, 1-15, 2014.

Sorlien, C. C., Luyendyk, B. P., Wilson, D. S., Decesari, R. C., Bartek, L. R., and Diebold, J. B.: Oligocene development of the West Antarctic Ice Sheet recorded in eastern Ross Sea strata, Geology, 35, 467-470, 2007.

Steinthorsdottir, M., Coxall, H., De Boer, A., Huber, M., Barbolini, N., Bradshaw, C., Burls, N., Feakins, S., Gasson, E., and Henderiks, J.: The Miocene: the future of the past, Paleoceanography and Paleoclimatology, 36, e2020PA004037, 2021.

Stickley, C., Brinkhuis, H., McGonigal, K., Chaproniere, G., Fuller, M., Kelly, D., Nürnberg, D., Pfuhl, H., Schellenberg, S., and Schönfeld, J.: Late Cretaceous–Quaternary biomagnetostratigraphy of ODP Sites 1168, 1170, 1171, and 1172, Tasmanian Gateway, Proceedings of the Ocean Drilling Program, Scientific Results, 1-57, doi:10.2973/odp.proc.sr.189.111.2004,

Stoll, H. M., Bolton, C., Jaggi, M., Martinez-Garcia, A., and Bernasconi, S. M.: Divergent estimates of Miocene to Pleistocene upper ocean temperatures in the South Atlantic Ocean from alkenone and coccolith clumped isotope proxies, Climate of the Past, 21, 2189-2203, 2025.

Stoll, H. M., Pena, L. D., Hernandez-Almeida, I., Guitián, J., Tanner, T., and Pälike, H.: Nonlinear increase in seawater 87Sr / 86Sr in the Oligocene to early Miocene and implications for climate-sensitive weathering, Clim. Past, 20, 25-36, 10.5194/cp-20-25-2024, 2024.

Thöle, L. M., Nooteboom, P. D., Hou, S., Wang, R., Nie, S., Michel, E., Sauermilch, I., Marret, F., Sangiorgi, F., and Bijl, P. K.: An expanded database of Southern Hemisphere surface sediment dinoflagellate cyst assemblages and their oceanographic affinities, Journal of Micropalaeontology, 42, 35-56, 2023.

Thomas, D. J. and Via, R. K.: Neogene evolution of Atlantic thermohaline circulation: perspective from Walvis Ridge, southeastern Atlantic Ocean, Paleoceanography, 22, 2007.

Van Peer, T. E., Liebrand, D., Taylor, V. E., Brzelinski, S., Wolf, I., Bornemann, A., Friedrich, O., Bohaty, S. M., Xuan, C., and Lippert, P. C.: Eccentricity pacing and rapid termination of the early Antarctic ice ages, Nature Communications, 15, 10600, 2024.

van Peer, T. E., Liebrand, D., Xuan, C., Lippert, P. C., Agnini, C., Blum, N., Blum, P., Bohaty, S. M., Bown, P. R., and Greenop, R.: Data report: revised composite depth scale and splice for IODP Site U1406, 2017.

Zachos, J., Pagani, M., Sloan, L., Thomas, E., and Billups, K.: Trends, rhythms, and aberrations in global climate 65 Ma to present, Science, 292, 686-693, 2001.